Materials Science in Semiconductor Processing 107 (2020) 104857

Contents lists available at ScienceDirect

Materials Science in Semiconductor Processing

journal homepage: http://www.elsevier.com/locate/mssp

Influence of working temperature on the structure and gas-sensing properties of γ-FeOOH submicron spheres

Vu Xuan Hien [a,*], Pham Tien Hung [b]

[a] School of Engineering Physics, Hanoi University of Science and Technology (HUST), 01 Dai Co Viet Street, Hanoi, Viet Nam
[b] School of Physics, Le Quy Don Technical University, Cau Giay District, Hanoi, Viet Nam

ARTICLE INFO

Keywords:
Metal
Iron oxides
Gas sensors
Microstructures

ABSTRACT

Iron oxyhydroxide (FeOOH) is an interesting material with major applications in water treatment. However, the gas-sensing properties of this nano-/micromaterial are not understood. Herein, we introduce a facile process for synthesizing submicron-sized γ-FeOOH spheres. The formation process of the γ-FeOOH phase after treatment is proposed, and the gas-sensing properties of the as-synthesized materials are investigated using NH_3, H_2S, NO_2, and SO_2. The influence of working temperature (from 25 °C to 300 °C) on material structure and gas-sensing performance is also studied and the gas-sensing process is explained and discussed.

1. Introduction

Iron oxyhydroxide (FeOOH) semiconductors, such as α-FeOOH, β-FeOOH, and γ-FeOOH, have narrow band gaps (E_g of ~2.1 eV) [1]. These materials have attracted considerable interest in the field of water splitting and as catalysts for degrading toxic pollutants under ultraviolet or visible light [2–5]. The nanostructures of these materials are commonly synthesized through various chemical approaches, such as low-temperature solution reaction [1], hydrothermal method [6], solvothermal synthesis [7] and solution oxidation method [8]. Amorphous FeOOH is grown on a Ni foil via one-pot hydrothermal synthesis [9]. Nevertheless, a direct synthesis procedure for FeOOH using Fe foil remains unavailable. A FeOOH semiconductor is treated as an immediate phase to form Fe_2O_3 before its gas-sensing properties are characterized [10,11]. Other studies investigated the sensing properties of FeOOH semiconductors modified/mixed with other materials [12,13], but the gas-sensing properties of FeOOH itself remain unclear.

In this study, γ-FeOOH microstructures were synthesized by oxidizing a Fe plate in NH_4OH at 40 °C. The gas-sensing properties of γ-FeOOH were characterized using a dynamical gas testing system at an operating temperature of 25–300 °C. The transformation of the gas-sensing properties and the material's phase/structure were analyzed by field emission scanning electron microscopy (FE-SEM) and X-ray diffraction (XRD) techniques, respectively.

2. Experimental

A commercial Fe plate (purity of 99.5%, thickness of 0.25 mm) was cut into 2 × 2 cm^2 plates. The plates were ground using grindstone and sandpaper for the removal of contaminants and oxides. The Fe plates were cleaned in a bath sonicator with acetone for 5 min, then dried under N_2 flow. The prepared plates were soaked in 25 mL of NH_4OH in a 100 mL Duran laboratory bottle. The Duran bottle was subsequently maintained in an oven at 40 °C for 4 days. After the treatment, the Duran bottle was placed in a bath sonicator for 5 min for the extraction of red powder on the Fe surface. The received red solution was washed with distilled water three times and centrifuged. Approximately 0.1 g of the obtained red powder was dispersed in 10 mL of ethanol in the bath sonicator for 5 min. The prepared solution (5 μL) was dropped on an interdigitated electrode (Pt electrode with a gap of 20 μm) with a micropipette for the fabrication of the sensor device.

The morphology and structure of the red powder were characterized by FE-SEM (JEOL JSM-7610 F) and XRD (X'Pert-Pro; λ = 1.5418 Å), respectively. Its chemical composition was determined through X-ray photoelectron spectroscopy (XPS; Quantera SXM). The binding energy data were calibrated using the C_{1s} signal of ambient hydrocarbons (C–H and C–C) at 284.6 eV. Gas-testing measurement was performed using a dynamic gas-testing system. Fig. 1 presents the structure of the electrode and the setup of our gas-sensing system. The sensor response is described as follows:

* Corresponding author.
E-mail address: hien.vuxuan@hust.edu.vn (V.X. Hien).

https://doi.org/10.1016/j.mssp.2019.104857
Received 16 August 2019; Received in revised form 1 November 2019; Accepted 18 November 2019
Available online 21 November 2019
1369-8001/

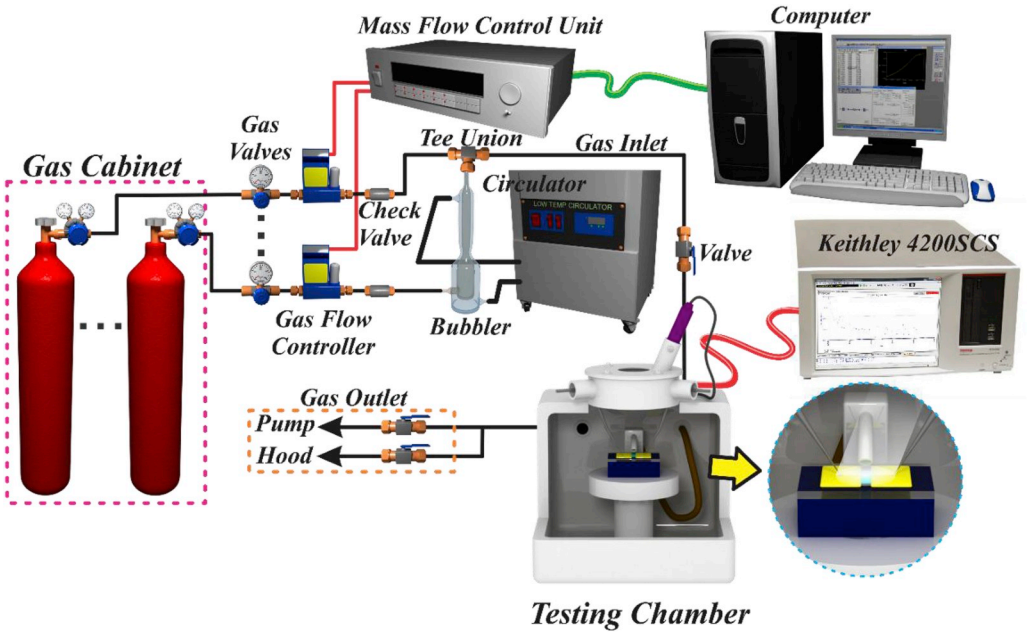

Fig. 1. Setup of the dynamic gas testing system.

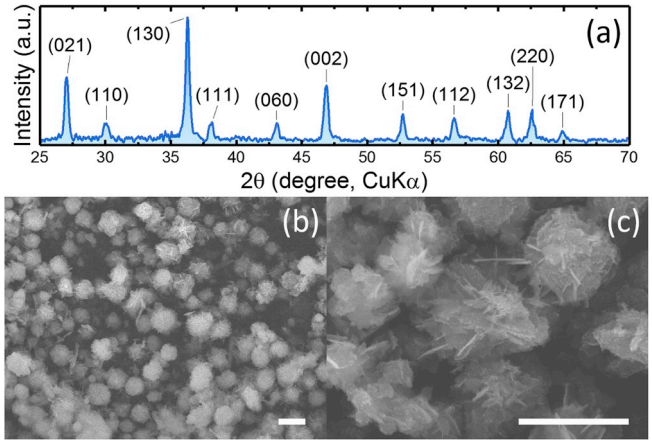

Fig. 2. (a) XRD pattern and (b–c) FE-SEM images of the red powder after treating the Fe plate in aqueous NH_4OH at 40 °C for 4 days. The scale bar is 1 μm.

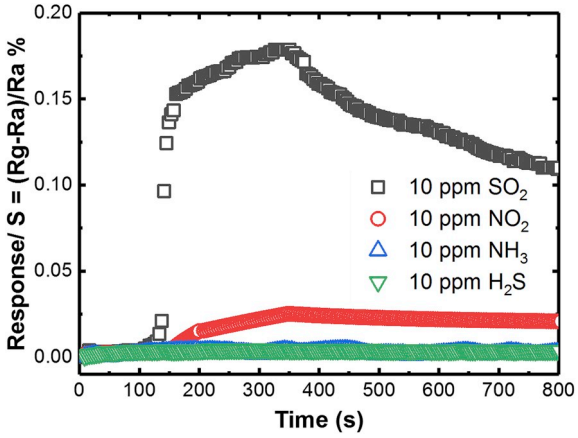

Fig. 3. Response/recovery curves of the γ-FeOOH device to various gases at 25 °C.

$$S = \frac{R_g - R_a}{R_a} \times 100\%, \quad (1)$$

where R_a and R_g are the sensor resistances of the device at a stable state in clean air and target gas, respectively. Response time is the duration at which 90% saturation response is achieved, and recovery time is the period required by the sensor to recover 90% of the maximum resistance when the target gas is off.

Before gas measurement, the device was maintained at 5 h operating temperature for the stabilization of the material structure. During the gas test, the total gas flux was 200 sccm, and the carrier gas was dry air.

3. Results and discussions

Fig. 2 shows the structure and morphology of the synthesized red powder. In the XRD pattern (Fig. 2a), all diffraction peaks matched the orthorhombic structure of γ-FeOOH [JCPDS file No. 98-002-7846, orthorhombic structure, space group *C m c m* (63)]. No phase was detected in the pattern. The crystalline size of the sample calculated using Sherer–Debye equation [14] at the diffraction peak of 36.2° is 22 nm. The FE-SEM images in Fig. 2b indicate that the γ-FeOOH sample is composed of submicron spheres. The sphere in Fig. 2c shows that the submicron spheres seem to be composed of many small plates arranged in different orientations. To the best of our knowledge, studies on the oxidation of metallic Fe in alkaline solution are rare. Nevertheless, the formation of γ-FeOOH during the treatment of Fe plate in NH_4OH may be similar to the oxidation of Cu in ammonia solution [15]. Metallic Fe can be oxidized and produce Fe^{2+} in the $[Fe(NH_3)_4]^{2+}$ complex:

$$Fe + \frac{1}{2}O_2 + H_2O + 4NH_3 \rightarrow [Fe(NH_3)_4]^{2+} + 2OH^-. \quad (2)$$

In ammonia solution, OH^- ions may swap NH_3 in the $[Fe(NH_3)_4]^{2+}$ complex to form $Fe(OH)_2$:

$$[Fe(NH_3)_4]^{2+} + 2OH^- \rightarrow Fe(OH)_2 + 4NH_3. \quad (3)$$

The hydroxide form of Fe in an alkaline solution can be transformed into a further stable phase *FeOOH* via the intermediate of $Fe(OH)_4^{2-}$, such as that occurring with $Cu(OH)_2$ [16–18]:

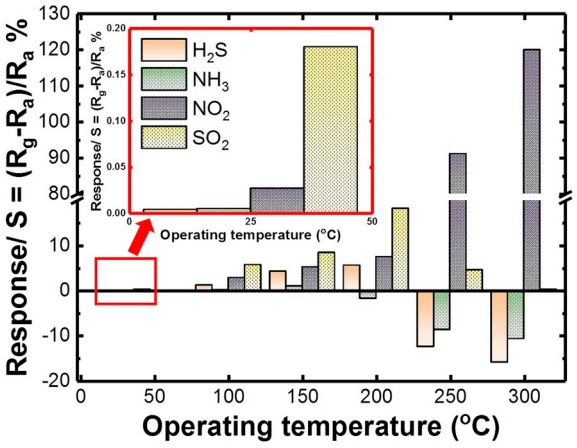

Fig. 4. Comparative bar chart of sensor response towards H_2S, NH_3, NO_2 and SO_2 at different operating temperatures. The gas concentration is 10 ppm.

$$Fe(OH)_2 + 2OH^- \rightarrow Fe(OH)_4^{2-}, \quad (4)$$

$$Fe(OH)_4^{2-} \rightarrow FeOOH + OH^- + H_2O. \quad (5)$$

here, the nanostructures of γ-FeOOH may be obtained through a reconstructive transformation involving a dissolution reaction followed by the precipitation of the $Fe(OH)_4^{2-}$ units, such as in the case of CuO [18–20].

The gas-sensing properties of the γ-FeOOH device were investigated using SO_2, NO_2, NH_3 and H_2S at 25 °C, as shown in Fig. 3. Amongst the target gases, the device was extremely sensitive towards 10 ppm SO_2, with a response of approximately 0.18%. Along with the low response value, the recovery time of the device at this temperature was gradual. This behavior may be explained by the slow adsorption/desorption of the target gas on the sensing sites at low temperatures, as mentioned in previous studies [21,22].

The bar chart in Fig. 4 summarises the influence of operating temperature on the sensor response towards H_2S, NH_3, NO_2, and SO_2. The optimal temperature of the device for detecting SO_2 was 200 °C with S of ~20%. Nevertheless, this device was increasingly sensitive towards NO_2 when the working temperature was increased. The highest response of the device to NO_2 was 120% at 300 °C. The gas-sensing behavior of the device seemed to reverse when the operating temperature reached 250 °C. The positive response ($R_g > R_a$) of the device towards NH_3 and H_2S completely changed to negative ($R_g < R_a$) at 250 °C, suggesting that the material phase did not remain when the working temperature increased. This phenomenon is reasonable because FeOOH is unstable and can transform to Fe_2O_3 at a temperature above 200 °C [23].

Fig. 5 shows the SO_2-sensing properties of the device at 200 °C. The response time modulation in Fig. 5a indicates repeatability under the operating conditions. The response and recovery times of this device to 10 ppm SO_2 were 28 and 38 s, respectively. Fig. 5b illustrates the influence of SO_2 concentration on the sensor response. Here, the response and recovery times did not vary when the SO_2 concentration changed. The detection limit of the sample to SO_2 was 1 ppm. The fluctuation of the response data to the SO_2 concentration was linear when the coefficient of determination (*R-square*) was 99.8% (Fig. 5c). Thus, the sensing mechanism during this test was not derived from complex processes. Device stability was examined at an operating temperature of 200 °C for 10 measurement days, as shown in Fig. 5d. The sensor response of the device slightly fluctuated after the 10-day test. The SO_2 sensing performance of the γ-FeOOH was compared with those of other nanomaterials in Table S1 (Supplemental Information).

The gas-sensing properties of a metal oxide semiconductor originate from the imperfect structure of the material [24]. The defects that occur on the material surface tend to adsorb various chemical species in the

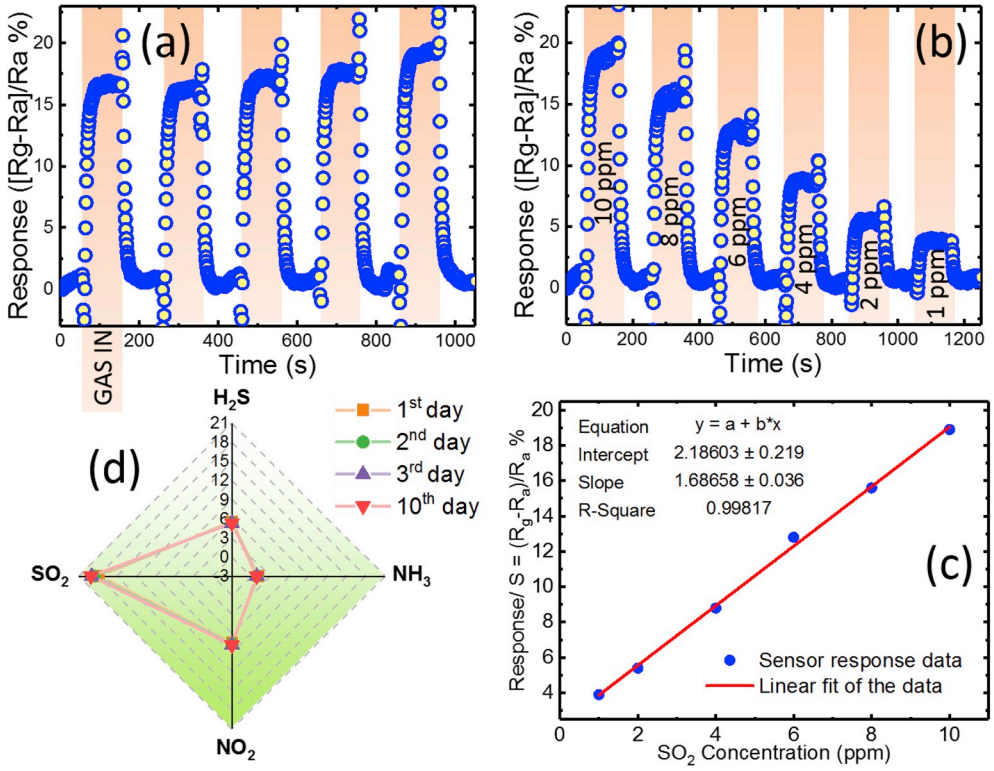

Fig. 5. (a) Modulation curve of the device to five-pulse SO_2 with 10 ppm concentration. (b) Response/recovery curves of the device to 1–10 ppm SO_2. (c) Fitting line of the response to SO_2 concentration data. (d) Radar chart of the sensor response to different target gases in different measurement days. The operating temperature is 200 °C.

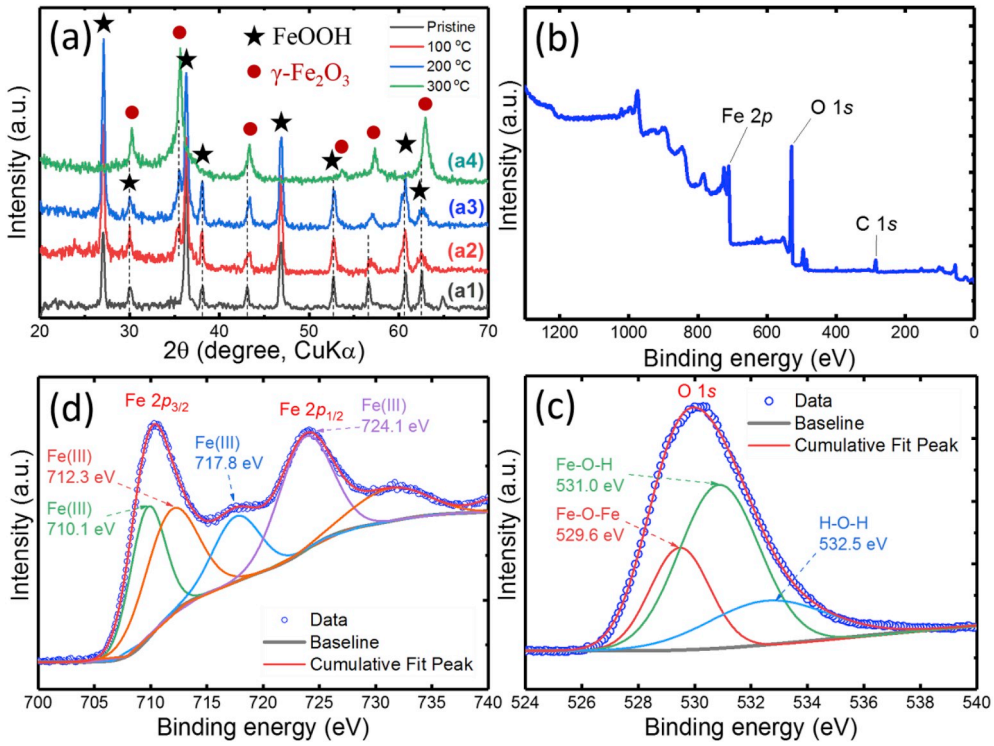

Fig. 6. (a) XRD patterns of the as-synthesized powder of γ-FeOOH (a1) without annealing process and after heat treatment at (a2) 100, (a3) 200 and (a4) 300 °C for 5 h. (b) XPS, (c) O 1*s* spectrum and (d) Fe 2*p* spectra of the γ-FeOOH powder annealed at 200 °C for 5 h.

environment, such as oxygen or water molecules. The adsorption of oxygen species on the surface of a metal oxide has been well studied, and the transitions of oxygen species through physisorption and chemisorption can be described as follows [25–28]:

$$O_2(gas) \leftrightarrow O_2(ads) \tag{6}$$

$$O_2(ads) + e^- \leftrightarrow O_2^-(ads)(T < 100^oC) \tag{7}$$

$$O_2^-(ads) + e^- \leftrightarrow 2O^-(ads)(100^oC < T < 300^oC) \tag{8}$$

$$O^-(ads) + e^- \leftrightarrow O^{2-}(ads)(T > 300^oC) \tag{9}$$

where '*ads*' is the adsorption. In n-type metal oxide semiconductors, such as SnO_2, ZnO and Fe_2O_3, the chemical bonding process involved in the formation of $O_2^-(ads)$, $O^-(ads)$ or $O^{2-}(ads)$ results in the withdrawal of electrons in the conduction band or in the formation or expansion of a depletion zone on a material surface (Eq. (7)) [29,30]. Inversely, the formation of oxygen adatoms on the surface of p-type metal oxide semiconductors, such as SnO and CuO, leads to the addition of holes in the valence band or the formulation/expansion of the accumulation zone near the material surface [31]:

$$O_2(ads) \leftrightarrow O_2^- + h^+(ads). \tag{10}$$

The oxygen adatoms in an n-type metal oxide can react with reducing gases, such as NH_3 and H_2S, as follows:

$$4NH_3(g) + 5O_2^{n-}(ads) \rightarrow 4NO + 6H_2O + 5ne^-, \tag{11}$$

$$2H_2S + 3O_2^{n-}(ads) \rightarrow 2H_2O + 2SO_2 + 3ne^-. \tag{12}$$

After the reactions, the released electrons can reduce material resistance ($R_g < R_a$). Inversely, the reducing gases can react with oxygen adatoms in a p-type metal oxide, leading to the increased resistance ($R_g > R_a$) of the sensing material. The free-electron generated in Eqs. (11–12) can recombine with the holes in the valence band of a p-type semiconductor, thereby increasing material resistance. These arguments indicate that our device presents the p-type semiconducting gas-sensing material and changes to the n-type sensing properties at operating temperatures below and above 200 °C, respectively. Therefore, the high response of the device to NO_2 above 200 °C may result from another oxide form of Fe, except FeO.

The phase transformation of γ-FeOOH under elevated temperature was characterized by XRD. Fig. 6a shows the XRD patterns of the γ-FeOOH powder after treatment at 100–300 °C for 5 h each. In the patterns of the samples treated at 100 and 200 °C, minor diffraction peaks that match γ-Fe_2O_3 were observed at 35.3° and 56.8° [JCPDS File No. 98–0.24-7034, cubic structure, space group *F d -3 m* (227)]. When the treatment temperature reached 300 °C, all the diffraction peaks of the γ-FeOOH were completely replaced with a set of peaks, which agreed with the cubic structure of γ-Fe_2O_3. XPS analysis was performed to characterize the chemical composition of the γ-FeOOH powder treated at 200 °C for 5 h. The survey spectrum shown in Fig. 6b indicates that Fe, O, and C are the main components in the sample. The O 1*s* spectrum of the sample is presented in Fig. 6c. In these data, one strong peak appeared, which is well deconvoluted into three peaks located at 529.6, 531.0 and 532.5 eV. These peaks can be assigned to Fe–O–Fe, Fe–O–H and H–O–H bonds, respectively [32–34]. The appearance of the Fe–O and Fe–O–H bonds suggests the existence of the FeOOH phase in the sample [35]. The deconvoluted peaks in the Fe 2*p* spectrum (Fig. 6d) are quite similar to that of the reference of Fe_2O_3 in which the separation between Fe $2p_{1/2}$ and Fe $2p_{3/2}$ peaks ($\Delta = 2p_{1/2} - 2p_{3/2}$) is 14 eV [36]. Based on these data, the gas-sensing properties of the device at 100–300 °C involved two possible structures: Fe_2O_3/γ-FeOOH (n/p-type structure) and γ-Fe_2O_3 (n-type structure). The sensing behavior of the Fe_2O_3/γ-FeOOH structure is possibly similar to that of the SnO_2/SnO structure, which is well studied [37,38]. Both structures presented p-type sensing properties at low temperatures and changed to n-type sensing properties when the operating temperature was increased [39]. When the Fe_2O_3/γ-FeOOH structure completely transformed into a γ-Fe_2O_3 phase at 300 °C, the sensing properties of the device showed n-type semiconducting sensing properties, such as those of other Fe_2O_3

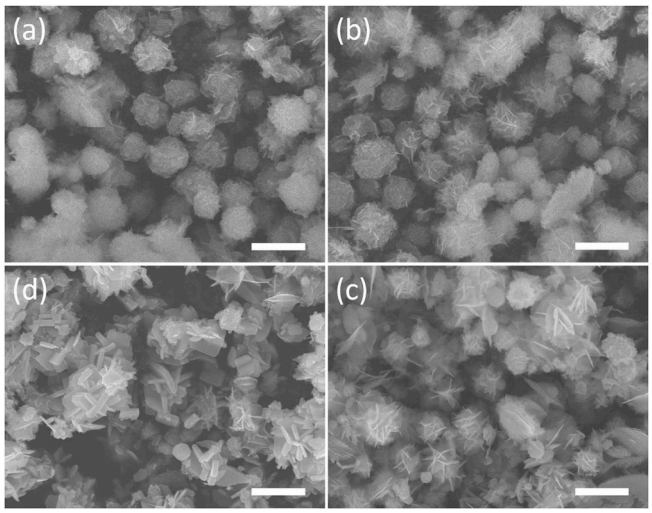

Fig. 7. (a) FE-SEM images of the red powder without annealing and after heat treatment at (b) 100, (c) 200 and (d) 300 °C for 5 h. The scale bar is 1 μm.

nanomaterials [40,41].

The oxidations of γ-FeOOH to γ-Fe_2O_3 may cause a change in the surface morphology of the γ-FeOOH submicron spheres, as captured in Fig. 7. At 100 °C, the surfaces of the spheres were rough because of the appearance of curvy nanowalls (Fig. 7b), which became large straight nanowalls at a treatment temperature of 200 °C (Fig. 7c). When the sample was treated at 300 °C for 5 h, the average thickness of the straight wall roughly increased from 10 nm to 100 nm (Fig. 7d). This change in morphology may affect sensing performance owing to the variation in the effective sensing area [42,43]. The decreased number of specific surface areas and active sites for gas sensing when the average thickness of the straight wall expands may reduce sensor response. Therefore, the phase change is possibly the major reason for the response upsurge of the sensor towards NH_3, H_2S, and NO_2 at 300 °C.

4. Conclusions

Submicron-sized γ-FeOOH rough spheres were synthesized by performing surface treatment on a Fe plate in aqueous NH_4OH at 40 °C. The formation process of the γ-FeOOH material was proposed and discussed based on Fe oxidation in an alkaline solution. The gas-sensing properties of the as-synthesized γ-FeOOH sample were investigated with target gases NH_3, H_2S, SO_2, and NO_2. The γ-FeOOH device could detect 10 ppm SO_2 at 25 °C, with a response of nearly 0.18%. The γ-FeOOH phase was partially transformed to Fe_2O_3 above 100 °C and completely changed to γ-Fe_2O_3 at 300 °C. This alteration led to the formation of curvy (at 100 °C) and straight (above 200 °C) nanowalls on the surface of the submicron spheres. Therefore, the gas-sensing data were confirmed to be from Fe_2O_3/γ-FeOOH and γ-Fe_2O_3 structures. Here, the p-type sensing behavior of γ-FeOOH was observed, and this material seemed extremely sensitive to SO_2 gas. The sensor response to 10 ppm SO_2 at 200 °C was nearly 20%, and the detection limit of the sample was 1 ppm. The response and recovery time of the device working at 200 °C was 28 and 38 s, respectively. γ-Fe_2O_3 was extremely sensitive to NO_2 at 300 °C, with a sensor response of roughly 120% (10 ppm NO_2).

Declaration of competing interest

The authors declare that they have no known competing financial interests or personal relationships that could have appeared to influence the work reported in this paper.

Acknowledgements

This research was funded by the Hanoi University of Science and Technology under Project No. T2018-PC-127.

Appendix A. Supplementary data

Supplementary data to this article can be found online at https://doi.org/10.1016/j.mssp.2019.104857.

References

[1] Y. Xiong, Y. Xie, S. Chen, Z. Li, Fabrication of self-supported patterns of aligned β-FeOOH nanowires by a low-temperature solution reaction, Chem. Eur J. 9 (2003) 4991–4996, https://doi.org/10.1002/chem.200305118.
[2] W.D. Chemelewski, H.C. Lee, J.F. Lin, A.J. Bard, C.B. Mullins, Amorphous FeOOH oxygen evolution reaction catalyst for photoelectrochemical water splitting, J. Am. Chem. Soc. 136 (2014) 2843–2850, https://doi.org/10.1021/ja411835a.
[3] M.C. Pereira, E.M. Garcia, A. Cândido Da Silva, E. Lorenon, J.D. Ardisson, E. Murad, J.D. Fabris, T. Matencio, T. De Castro Ramalho, M.V.J. Rocha, Nanostructured δ-FeOOH: a novel photocatalyst for water splitting, J. Mater. Chem. 21 (2011) 10280–10282, https://doi.org/10.1039/c1jm11736j.
[4] H. Li, W. Li, Y. Zhang, T. Wang, B. Wang, W. Xu, L. Jiang, W. Song, C. Shu, C. Wang, Chrysanthemum-like α-FeOOH microspheres produced by a simple green method and their outstanding ability in heavy metal ion removal, J. Mater. Chem. 21 (2011) 7878–7881, https://doi.org/10.1039/c1jm10979k.
[5] B. Wang, H. Wu, L. Yu, R. Xu, T.T. Lim, X.W. Lou, Template-free formation of uniform urchin-like α-FeOOH hollow spheres with superior capability for water treatment, Adv. Mater. 24 (2012) 1111–1116, https://doi.org/10.1002/adma.201104599.
[6] A.R. Amani-Ghadim, S. Alizadeh, F. Khodam, Z. Rezvani, Synthesis of rod-like α-FeOOH nanoparticles and its photocatalytic activity in degradation of an azo dye: empirical kinetic model development, J. Mol. Catal. A Chem. 408 (2015) 60–68, https://doi.org/10.1016/j.molcata.2015.06.037.
[7] Y. Zhang, P. Yan, Q. Wan, K. Wu, N. Yang, Morphology-dependent electrochemistry of FeOOH nanostructures, Electrochem. Commun. 68 (2016) 10–14, https://doi.org/10.1016/j.elecom.2016.04.007.
[8] Y. Ni, X. Ge, H. Liu, Z. Zhang, Q. Ye, F. Wang, Synthesis and characterization of α-FeO(OH) nano-rods in situ via a solution-oxidation, Mater. Lett. 49 (2001) 185–188, https://doi.org/10.1016/S0167-577X(00)00365-7.
[9] L. Yang, Y. Liu, J. Li, G. Du, One-pot hydrothermal synthesis of amorphous FeOOH on Ni foam for high performance supercapacitors, J. Alloy. Comp. 763 (2018) 134–140, https://doi.org/10.1016/j.jallcom.2018.05.305.
[10] X. Rao, X. Su, C. Yang, J. Wang, X. Zhen, D. Ling, From spindle-like β-FeOOH nanoparticles to α-Fe_2O_3 polyhedral crystals: shape evolution, growth mechanism and gas sensing property, CrystEngComm 15 (2013) 7250–7256, https://doi.org/10.1039/c3ce40430g.
[11] B. Liu, L. Gao, F. Zhou, G. Duan, Preferentially epitaxial growth of β-FeOOH nanoflakes on SnO_2 hollow spheres allows the synthesis of SnO_2/α-Fe_2O_3 heterostructured nanocomposites with enhanced gas sensing performance for dimethyl disulfide, Sens. Actuators B Chem. 272 (2018) 348–360, https://doi.org/10.1016/j.snb.2018.06.002.
[12] M.M. Doroodmand, S. Nasresfahani, M.H. Sheikhi, Fabrication of ozone gas sensor based on FeOOH/single walled carbon nanotube-modified field effect transistor, Int. J. Environ. Anal. Chem. 93 (2013) 946–958, https://doi.org/10.1080/03067319.2012.717269.
[13] T. Zhu, W.L. Ong, L. Zhu, G.W. Ho, TiO_2 fibers supported β-FeOOH nanostructures as efficient visible light photocatalyst and room temperature sensor, Sci. Rep. 5 (2015) 10601, https://doi.org/10.1038/srep10601.
[14] Harold P. Klug, Leroy E. Alexander, X-ray Diffraction Procedures for Polycrystalline and Amorphous Materials, John Wiley & Sons, 1974.
[15] S. Anandan, X. Wen, S. Yang, Room temperature growth of CuO nanorod arrays on copper and their application as a cathode in dye-sensitized solar cells, Mater. Chem. Phys. 93 (2005) 35–40, https://doi.org/10.1016/j.matchemphys.2005.02.002.
[16] Y. Li, D. Cao, Y. Liu, R. Liu, F. Yang, J. Yin, G. Wang, CuO nanosheets grown on cupper foil as the catalyst for H_2O_2 electroreduction in alkaline medium, Int. J. Hydrogen Energy 37 (2012) 13611–13615, https://doi.org/10.1016/j.ijhydene.2012.01.038.
[17] Y. Zhao, J. Zhao, Y. Li, D. Ma, S. Hou, L. Li, X. Hao, Z. Wang, Room temperature synthesis of 2D CuO nanoleaves in aqueous solution, Nanotechnology 22 (2011) 115604, https://doi.org/10.1088/0957-4484/22/11/115604.
[18] Y. Cudennec, A. Lecerf, The transformation of $Cu(OH)_2$ into CuO, revisited, Solid State Sci. 5 (2003) 1471–1474, https://doi.org/10.1016/j.solidstatesciences.2003.09.009.
[19] T. Soejima, K. Takada, S. Ito, Alkaline vapor oxidation synthesis and electrocatalytic activity toward glucose oxidation of CuO/ZnO composite nanoarrays, Appl. Surf. Sci. 277 (2013) 192–200, https://doi.org/10.1016/j.apsusc.2013.04.024.
[20] C. Lu, L. Qi, J. Yang, D. Zhang, N. Wu, J. Ma, Simple template-free solution route for the controlled synthesis of $Cu(OH)_2$ and CuO nanostructures, J. Phys. Chem. B 108 (2004) 17825–17831, https://doi.org/10.1021/jp046772p.

[21] H. Li, W. Xie, B. Liu, C. Wang, Y. Wang, X. Duan, Q. Li, T. Wang, Gas modulating effect in room temperature ammonia sensing, Sens. Actuators B Chem. 242 (2017) 404–411, https://doi.org/10.1016/j.snb.2016.11.028.
[22] L. Ghimpu, O. Lupan, V. Postica, J. Strobel, L. Kienle, M.I. Terasa, M. Mintken, I. Tiginyanu, J. Marx, B. Fiedler, R. Adelung, Individual CdS-covered aerographite microtubes for room temperature VOC sensing with high selectivity, Mater. Sci. Semicond. Process. 100 (2019) 275–282, https://doi.org/10.1016/j.mssp.2019.05.013.
[23] B. Tang, G. Wang, L. Zhuo, J. Ge, L. Cui, Facile route to α-FeOOH and α-Fe_2O_3 nanorods and magnetic property of α-Fe_2O_3 nanorods, Inorg. Chem. 45 (2006) 5196–5200, https://doi.org/10.1021/ic060097b.
[24] G. Korotcenkov, Metal oxides for solid-state gas sensors: what determines our choice? Mater. Sci. Eng. B. 139 (2007) 1–23, https://doi.org/10.1016/j.mseb.2007.01.044.
[25] A. Bielański, J. Haber, Oxygen in catalysis on transition metal oxides, Catal. Rev. 19 (1979) 1–41, https://doi.org/10.1080/03602457908065099.
[26] S. Chang, Oxygen chemisorption on tin oxide: correlation between electrical conductivity and EPR measurements, J. Vac. Sci. Technol. 17 (1980) 366–369, https://doi.org/10.1116/1.570389.
[27] D. Kohl, Surface processes in the detection of reducing gases with SnO_2-based devices, Sens. Actuators 18 (1989) 71–113, https://doi.org/10.1016/0250-6874(89)87026-X.
[28] R. Xu, L.X. Zhang, M.W. Li, Y.Y. Yin, J. Yin, M.Y. Zhu, J.J. Chen, Y. Wang, L.J. Bie, Ultrathin SnO_2 nanosheets with dominant high-energy {001} facets for low temperature formaldehyde gas sensor, Sens. Actuators B Chem. (2019) 186–194, https://doi.org/10.1016/j.snb.2019.03.012.
[29] C. Wang, L. Yin, L. Zhang, D. Xiang, R. Gao, Metal oxide gas sensors: sensitivity and influencing factors, Sensors 10 (2010) 2088–2106, https://doi.org/10.3390/s100302088.
[30] N. Barsan, D. Koziej, U. Weimar, Metal oxide-based gas sensor research: how to? Sens. Actuators B Chem. 121 (2007) 18–35, https://doi.org/10.1016/J.SNB.2006.09.047.
[31] M. Hübner, C.E. Simion, A. Tomescu-Stănoiu, S. Pokhrel, N. Bârsan, U. Weimar, Influence of humidity on CO sensing with p-type CuO thick film gas sensors, Sens. Actuators B Chem. 153 (2011) 347–353, https://doi.org/10.1016/j.snb.2010.10.046.
[32] Y.X. Zhang, Y. Jia, A facile solution approach for the synthesis of akaganéite (β-FeOOH) nanorods and their ion-exchange mechanism toward As(V) ions, Appl. Surf. Sci. 290 (2014) 102–106, https://doi.org/10.1016/j.apsusc.2013.11.007.
[33] J. Liu, M. Zheng, X. Shi, H. Zeng, H. Xia, Amorphous FeOOH quantum dots assembled mesoporous film anchored on graphene nanosheets with superior electrochemical performance for supercapacitors, Adv. Funct. Mater. 26 (2016) 919–930, https://doi.org/10.1002/adfm.201504019.
[34] T. Wang, Z. Jiang, K.H. Chu, D. Wu, B. Wang, H. Sun, H.Y. Yip, T. An, H. Zhao, P. K. Wong, X-shaped α-FeOOH with enhanced charge separation for visible-light-driven photocatalytic overall water splitting, ChemSusChem 11 (2018) 1365–1373, https://doi.org/10.1002/cssc.201800059.
[35] T. Yang, L. Meng, S. Han, J. Hou, S. Wang, X. Wang, Simultaneous reductive and sorptive removal of Cr(VI) by activated carbon supported β-FeOOH, RSC Adv. 7 (2017) 34687–34693, https://doi.org/10.1039/c7ra06440c.
[36] H. Lv, H. Zhao, T. Cao, L. Qian, Y. Wang, G. Zhao, Efficient degradation of high concentration azo-dye wastewater by heterogeneous Fenton process with iron-based metal-organic framework, J. Mol. Catal. A Chem. 400 (2015) 81–89, https://doi.org/10.1016/j.molcata.2015.02.007.
[37] L. Li, C. Zhang, W. Chen, Fabrication of SnO_2 –SnO nanocomposites with p–n heterojunctions for the low-temperature sensing of NO_2 gas, Nanoscale 7 (2015) 12133–12142, https://doi.org/10.1039/C5NR02334C.
[38] V.X. Hien, J.-H. Lee, J.-J. Kim, Y.-W. Heo, Structure and NH_3 sensing properties of SnO thin film deposited by RF magnetron sputtering, Sens. Actuators B Chem. 194 (2014) 134–141, https://doi.org/10.1016/J.SNB.2013.12.086.
[39] V.X. Hien, Y.-W. Heo, Effects of violet-, green-, and red-laser illumination on gas-sensing properties of SnO thin film, Sens. Actuators B Chem. 228 (2016) 185–191, https://doi.org/10.1016/J.SNB.2015.12.105.
[40] H.-J. Zhang, F.-N. Meng, L.-Z. Liu, Y.-J. Chen, Convenient route for synthesis of alpha-Fe_2O_3 and sensors for H_2S gas, J. Alloy. Comp. 774 (2019) 1181–1188, https://doi.org/10.1016/j.jallcom.2018.09.384.
[41] Y. Guo, X. Tian, X. Wang, J. Sun, Fe_2O_3 nanomaterials derived from Prussian blue with excellent H_2S sensing properties, Sens. Actuators B Chem. 293 (2019) 136–143, https://doi.org/10.1016/j.snb.2019.04.027.
[42] Y. Deng, Y. Deng, Semiconducting metal oxides: morphology and sensing performance, in: Semicond. Met. Oxides Gas Sens, Springer Singapore, Singapore, 2019, pp. 53–75, https://doi.org/10.1007/978-981-13-5853-1_3.
[43] V.X. Hien, J.-L. You, K.-M. Jo, S.-Y. Kim, J.-H. Lee, J.-J. Kim, Y.-W. Heo, H_2S-sensing properties of Cu_2O submicron-sized rods and trees synthesized by radio-frequency magnetron sputtering, Sens. Actuators B Chem. 202 (2014) 330–338, https://doi.org/10.1016/j.snb.2014.05.070.